Modeling Microglial Responses to Genetic Perturbations in Alzheimer's Disease

Elyssa Nguyen, Seungyoon Blenda Yu

Abstract

This project investigates the factors that determine whether microglia, the brain's resident immune cells, promote clearance of Alzheimer's disease (AD) pathology or contribute to disease progression. The first workflow (Aim 1) tests the inverse association between glioblastoma (GBM) and AD by introducing oncogenic mutations into postnatal APP/PS1 mice via postnatal electroporation, alongside establishing primary microglia and bone-marrow-derived macrophage (BMDM) culture and engraftment protocols. The second workflow (Aim 2) models clonal hematopoiesis of indeterminate potential (CHIP)-associated mutations (TET2, DNMT3A, and ASXL1) in a human embryonic stem cell (hESC)-derived microglia-like cell (iMGL) model incorporated into cerebral organoids. Two parallel CRISPR delivery strategies, RNP electroporation and Cas9/mCherry lentiviral gRNA delivery, are being developed to test whether these mutations alter microglial proliferative, inflammatory, or disease-associated phenotypes. This summer's work was primarily foundational, focusing on establishing stem cell maintenance and differentiation protocols, developing a literature-grounded candidate gene list to guide target selection, and optimizing the experimental pipelines for both aims. Together, these workflows establish complementary in vivo and in vitro systems for investigating how specific genetic and cellular perturbations influence microglial responses to AD pathology.

1. INTRODUCTION

1.1 From a Metabolic Question to a Microglial One

This project was originally proposed to test a specific hypothesis that midlife obesity leaves a lasting epigenetic "memory" in microglia as evidenced by work showing that metabolic stress can reprogram immune cell gene expression even after the stress is removed, and that this memory primes the brain toward the kind of chronic neuroinflammation seen in AD (Hinte et al., 2024; Dong et al., 2024). Over the first week of the fellowship, however, the project's direction shifted in response to the host lab's ongoing priorities and available models, moving away from a diet-induced obesity paradigm and toward two workflows. Although the specific risk factor under investigation changed, the underlying question did not: what determines whether a microglial cell's response to AD pathology is protective or harmful? The remainder of this introduction discusses how each workflow arrived at that same question from a different starting point, before turning to the literature review used to select candidate genes for both.

1.2 Aim 1: An Inverse Relationship Between Cancer and Alzheimer's Disease

The first workflow builds on a well-documented but counterintuitive epidemiological pattern that cancer and AD are inversely associated. Both diseases reflect a breakdown in normal cell-cycle control, but in opposite directions. AD involves neuronal death, while cancer involves uncontrolled proliferation (Li et al., 2014). Mature neurons are normally post-mitotic, meaning they permanently exit the cell cycle after differentiating. In AD, neurons appear to attempt re-entry into the cell cycle but fail to complete division, in part because they lack functional topoisomerase II and instead rely on an error-prone DNA repair enzyme not built for full genome replication. The resulting DNA damage during this stalled division is proposed to trigger amyloid and tau pathology (Kruman et al., 2004). Cancer cells, by contrast, successfully complete this same re-entry allowing them to proliferate rapidly, eventually causing the cancer to spread (Mercadante & Kasi, 2023).

One proposed shared pathway underlying both outcomes is PI3K/Akt/mTOR signaling, which is normally activated by metabolic and oxidative stress and drives cells to re-enter the cell cycle while blocking autophagy (the process that clears damaged proteins, including amyloid-β and misfolded tau). The severity of the stress may determine which disease results as a fast-growing tumor consumes so much local energy that it activates a different pathway (AMPK-FOXO) that blocks mTOR and protects nearby tissue from cell-cycle re-entry which in effect, shields the body from AD-like pathology, whereas the slower, chronic oxidative stress of aging instead favors the PI3K/Akt/mTOR route directly (Majd et al., 2019). Consistent with this model, a retrospective analysis of the SEER cancer registry found that glioblastoma was substantially rarer than expected in patients who died of AD (odds ratio 0.19), suggesting the two diseases may actively suppress one another in the brain (Xia et al., 2023).

This association, however, is purely correlational, and no study has directly tested it by introducing an oncogenic mutation into an established AD mouse model. This workflow addresses that gap with APP/PS1 mice, the standard model for early amyloid plaque formation, are used as the background for postnatal electroporation of cancer-driver mutations into the subventricular zone, testing directly whether oncogenic transformation can mechanistically protect surrounding brain tissue from AD pathology.

1.3 Aim 2: Clonal Hematopoiesis as a Second Route Into Microglial Biology

The second workflow began from a different, and initially contradictory, line of evidence involving clonal hematopoiesis of indeterminate potential (CHIP), an aging-related condition in which blood stem cells acquire mutations that give them a modest growth advantage, allowing a mutant clone to gradually dominate the blood-forming stem cell pool. When this occurs in one of a small set of recurrently mutated genes (most often DNMT3A or TET2, less often ASXL1), the

condition is specifically termed CHIP (Steensma et al., 2015), and it is already an established risk factor for cardiovascular disease through the chronic inflammation produced by CHIP-mutant monocytes and macrophages (Jaiswal & Libby, 2020). Huang et al. proposed that these same mutant blood cells can cross a weakened blood-brain barrier during aging or early AD and differentiate into microglia-like cells inside the brain (Huang et al., 2026).

Whether this is good or bad for the brain is genuinely unresolved. Early, lower-depth sequencing studies found no association, or even a protective association, between CHIP and AD (Bouzid et al., 2023; Kessler et al., 2022). Using much deeper sequencing capable of detecting far smaller mutant clones, Huang et al. instead found more CHIP mutations in AD brains than controls, localized specifically to microglia, and showed using isogenic CRISPR-edited stem cell lines differing by a single CHIP mutation that the mutation alone was sufficient to push microglia-like cells toward a disease-associated, proliferative state, independent of any AD pathology (Huang et al., 2026). Bouzid et al. reached the opposite conclusion in their own cohort as CHIP carriers had lower odds of AD, an association that held up under Mendelian randomization and correlated with less amyloid and tau pathology at autopsy though this protective signal was present only in larger mutant clones and disappeared for the smaller clones that drove Huang et al.'s risk signal, suggesting the two studies may be describing different populations of mutant cells rather than directly contradicting one another. Bouzid et al. proposed an opposite mechanism entirely and hypothesized that as native microglia lose phagocytic capacity with age, mutant blood cells may infiltrate the brain to help clear amyloid rather than to attack it as Huang had suggested (Bouzid et al., 2023).

Because this workflow requires selecting specific genes to model in an isogenic CRISPR system, the CHIP literature was reviewed at the level of individual driver genes (TET2, DNMT3A, ASXL1) to weigh the evidence for each gene's role in microglial activation and AD risk specifically. This evidence, along with the genes identified in Section 1.4 below, is summarized in Table 1.

Table 1. Candidate Gene Reference Tables: CHIP × AD/GBM Microglial Screen

1.4 When Does Microglia Become Harmful in AD?

Both workflows converge on the same underlying cell type and the same open question: what determines whether microglia help clear AD pathology or make it worse? This is not a minor detail as genome-wide association studies (GWAS) have identified more than 80 genetic risk loci for AD, and roughly a quarter of these are genes expressed almost exclusively by microglia, indicating that microglia actively drive disease rather than simply reacting to it (Heneka et al., 2024). What the field lacks is a reliable way to identify, at the level of an individual cell, which microglia are doing the damage.

Part of the difficulty is that microglial "activation" is not one consistent thing. The same core disease-associated microglia (DAM) gene signature looks different depending on what triggered it. In a paper by Musuda et al., comparing three different mouse disease models produced three distinct DAM-like states rather than one shared program (Masuda et al., 2020). Microglia also share several marker genes with other, related immune cells living in the tissue around the brain rather than inside it, which older studies often failed to distinguish (Amann & Prinz, 2026). Even the best-understood microglial pathway in AD, the TREM2/APOE axis, looks meaningfully different between mice and humans, with human microglia showing far more state diversity overall (Heneka et al., 2024). Together, this literature suggests that no single marker gene or single disease model can reliably identify "critical" microglia which is why this project prioritized studies that defined a microglial state functionally (by behavior, physical location, or lineage) rather than by marker gene alone.

Three studies were especially informative. Grubman et al. used a fluorescent dye that labels microglia only after they have physically engulfed amyloid plaque, allowing them to define an active, phagocytic microglial state by direct behavior. These cells switched on a lipid-handling gene program (TREM2, APOE) and a program controlled by HIF1α, a gene the authors then directly tested by knocking it down and overexpressing it. Doing so was shown to reduce and increase phagocytosis accordingly (Grubman et al., 2021). Ardura-Fabregat et al. used permanent cell labeling to prove that resting microglia can convert into plaque-associated microglia over several weeks, and found that once converted, these cells become comparatively unresponsive to further stimuli while also showing that several standard DAM markers (Clec7a, Apoe, Axl, P2ry12) failed to distinguish plaque-associated from non-plaque-associated microglia in their model, even though a different marker pair (CD11c, Tmem119) worked well (Ardura-Fabregat et al., 2025). Lu et al., who worked with human brain tissue, found that the amyloid burden alone did not distinguish demented from non-demented elderly patients. Instead, tau did. They identified a specific transition point at which the microglial response shifts from an early, amyloid-driven TREM2/APOE program to a later, more aggressive antigen-presentation program that switches on only once tau accumulates (Lu et al., 2026). A follow-up study found the same aggressive signature in human tissue but linked it to microglia being in direct physical contact with a plaque rather than to tau, leaving open whether plaque contact, tau, or both actually drive this switch (Wood et al., 2025).

It is clear that in order to design a sound study, microglial states should be defined functionally. Across these studies, a recurring, relatively small set of genes and pathways kept resurfacing as markers of the shift from a helpful to a harmful microglial state. These findings formed the basis of the candidate gene list used to guide this project's experimental design, summarized in Table 2.

Table 2. Relevant Literature Investigating Target Genes for AD Microglial States

1.5 Specific Aims Summarized

Aim 1 (Cancer × AD): To mechanistically test the epidemiologically observed inverse association between GBM and AD by introducing oncogenic driver mutations into the neural stem/progenitor cells of postnatal APP/PS1 mice via postnatal electroporation. In parallel, this workflow establishes protocols for isolating and culturing primary myeloid lineage cells (primary microglia, with bone-marrow-derived macrophages as a backup) from wild-type mice for engraftment into microglia-depleted host animals, with planned progression toward glioblastoma-bearing and, eventually, AD mouse models.

Aim 2 (CHIP × AD): To model CHIP-associated mutations (TET2, DNMT3A, ASXL1) in an isogenic human hESC background, differentiate mutant and wild-type lines through a hematopoietic progenitor intermediate into induced microglia-like cells (iMGLs), and incorporate these iMGLs into AD-model cerebral organoids, testing whether these mutations alone are sufficient to drive a disease-associated, proliferative, or inflammatory microglial phenotype, and whether an AD organoid environment amplifies mutant clone survival or inflammatory output. Two parallel CRISPR-based workflows converge on this endpoint:
(1) direct CRISPR RNP electroporation for a single targeted mutation
(2) a Cas9/mCherry-expressing line with pooled lentiviral gRNA delivery, providing a scalable, pooled-screening approach.

2. METHODS

2.1 Aim 1: Cancer × AD In Vivo Model

2.1.1 Postnatal Electroporation of Oncogenic Constructs

Oncogenic driver constructs were introduced into the neural stem/progenitor cell population lining the lateral ventricles of postnatal day 1 (P1) APP/PS1 and wild-type (WT) B6J mouse pups via postnatal intraventricular electroporation. The plasmid approach was adapted from the precancerous GBM model previously established by the laboratory, in which a Cre-containing CRISPR/Cas9 vector is electroporated into the lateral ventricle to introduce oncogenic alterations into neonatal neural stem cells (Kim et al., 2025). In the established model, the pU6-sgTP53-pU6-sgPTEN-CBh-Cas9-P2A-Cre plasmid targets Trp53 and Pten while expressing Cas9 and Cre. In that model, Cre additionally activates an LSL-EGFRvIII allele already present in the mouse genome, producing the combination of oncogenic alterations used to generate the GBM model. However, neither the APP/PS1 nor WT B6J mice used in the present pilot carry the LSL-EGFRvIII allele so the present experiment does not reproduce the full EGFRvIII-based

GBM model but as a pilot will evaluate whether the delivered oncogenic CRISPR construct produces detectable cellular proliferation in the APP/PS1 and WT backgrounds, providing an initial assessment of the system before longer-term tumor-development studies that can test the relationship between glioblastoma development and Alzheimer's disease pathology.

2.1.2 Tissue Preparation and Immunohistochemistry Staining

Electroporated mice (n = 10) were transcardially perfused at 10 weeks of age with phosphate-buffered saline (PBS) followed by ~20 mL of 4% paraformaldehyde (PFA), consistent with standard transcardial perfusion protocols for mouse brain tissue fixation (Gage et al., 2012). Brains were extracted and post-fixed in 4% PFA, then cryoprotected by immersion in a 30% sucrose solution at 4°C until the tissue sank.

After cryoprotection, brains were embedded in optimal cutting temperature (OCT) compound and sectioned coronally on a Cryostat Lecia at -20°C. Sectioning was done with the aid of the Allen Lab Coronal Brain Atlas began once the fiber tracts became visible as this is considered the anterior boundary of hippocampal tissue (Allen Brain Atlas, 2011). Sections were collected from the frontal cortex, through the hippocampus, and into the visual cortex. The cerebellum was excluded from the collection. More hippocampal regions were collected relative to the other brain regions. Intact, undamaged sections were selected for later immunofluorescence staining and were put into a 24-well plate containing PBS. The free-floating brain sections were then blocked and permeabilized in an IHC blocking buffer for 1 hour at room temperature on an orbital shaker, followed by incubation in primary antibodies which were diluted in the IHC blocking buffer, overnight at 4°C on a shaker. Two antibody panels were used to characterize cellular proliferation and its relationship to neural and glial populations. The first panel consisted of mouse anti-Ki67, rabbit anti-amyloid-β (Rb-AB), and goat anti-Iba1, while the second consisted of mouse anti-NeuN, rabbit anti-Iba1, and rat anti-Ki67. Ki67 was used as a marker of cellular proliferation, Iba1 as a marker of microglia, NeuN as a neuronal marker, and amyloid-β staining to assess plaque pathology. The use of two panels allowed proliferation to be examined in relation to different cellular and pathological features of the brain.

The following day, sections were washed in PBS and put on the orbital shaker (3 x 10 min) and were incubated in secondary antibodies. There were two panels once again with the first panel being anti-mouse-alexa-fluor-647, anti-alexa-rabbit-fluor-488, and anti-alexa-goat-fluor-594. The second panel was anti-mouse-alexa-fluor-647, anti-alexa-rabbit-fluor-488, and anti-alexa-rat-fluor-594. Both panels were diluted in the IHC blocking buffer for 1 hour at room temperature on the orbital shaker protected from light. Sections were counterstained with DAPI to label nuclei, washed, and put on slides for fluorescence imaging.

Because the APP/PS1 and WT B6J mice used in this pilot lack the LSL-EGFRvIII allele required for the full GBM model described by Kim et al., the present experiment was not expected to reproduce the same tumor-development trajectory. H&E staining would provide a complementary assessment of tissue morphology and overt tumor formation but at 10 weeks, morphological changes may be too subtle to reliably identify established cancerous tissue. With the lab's existing GBM plasmid, tumors are expected to be seen by week 20. Because APP/PS1 amyloid pathology itself also progresses gradually as plaque deposition in this model typically becomes detectable from ~6 months of age onward, a 10-week endpoint precedes the developmental window in which any interaction between tumor growth and amyloid pathology would be expected to manifest. Later cohorts may require longer follow-up to determine whether proliferative changes progress to a recognizable tumor phenotype and to assess interactions with amyloid pathology.

2.1.3 Primary Microglia Isolation and Engraftment Pilot

Depletion and replacement of endogenous microglia with an exogenous population is planned as a later step of the electroporation-based GBM model (Section 2.1.1) as once oncogenic electroporation produces the tumor, amyloid-depositing host, endogenous microglia in the same mouse would be depleted and substituted with exogenous donor microglia which would allow the behavior of a trackable microglia population to be studied in a GBM/AD microenvironment. Because this strategy has not been established in the lab, a pilot was done in a non-electroporated host to test the feasibility of microglia isolation, viral labeling, depletion, and engraftment independent of the electroporation part of the project before being able to combine both.

Donor microglia was isolated from wild-type mouse cortical tissue then a mixed glial culture of Minimum Essential Media (MEM) with 10% Fetal Bovine Serum (FBS) was made . Briefly, the cortical tissue is mechanically and enzymatically dissociated and plated on poly-D-lysine (PDL) or poly-L-ornithine coated plates where a confluent astrocyte monolayer forms over 9-10 days and supports the proliferation of a loose microglia population. This is cultured in DMEM (high glucose), 10% FBS, and 1% penicillin-streptomycin and a mechanical orbital "shake-off" method is used over the course of 2 hours at 180 rpm, detaching the microglia from the astrocyte layer and is expected to yield 2-6 million microglia per T175 flask (Ni & Aschner, 2010; R&D Systems, n.d.).

To track donor cell identity and clonal contribution after transplantation, isolated primary microglia were transduced with a barcode (BC) lentiviral vector co-expressing a U6-driven single guide RNA as this served as a sequenceable clonal barcode. The lentiviral vector also has a constitutive hPGK-EGFP reporter for identifying and quantifying transduced cells. Transduction efficiency was tested across three multiplicities of infection (MOI 0.3, 1, and 3) and two serum conditions (5% and 10%), alongside a non-barcoded control (CTL) lentivirus, and

quantified by flow cytometry for the percentage of GFP+ cells (VectorBuilder, n.d.). A range of MOIs was tested to determine an appropriate lentiviral concentration for donor-cell labeling. This optimization was important because the downstream clonal-tracking approach relies on each cell receiving a single lentiviral barcode. At higher levels of transduction, individual cells may receive multiple viral integrations, making it difficult to associate a barcode with a single original cell clone (Cellecta, n.d.). Previous studies have also shown that lentiviral transduction efficiency in microglia increases with increasing MOI (Maes et al., 2019). Serum concentration was tested as a second variable because serum can affect microglial viability, activation state, and phenotype in culture, and may therefore influence lentiviral transduction efficiency (Dan & Zheng, 2025). Together, these optimization experiments were used to identify transduction conditions that provided efficient labeling while minimizing multiple viral integrations and undesirable effects on microglial state. The BC lentivirus chosen was Serum 10% with an MOI of 0.3.

The host mice then underwent pharmacological depletion of exogenous microglia via the dietary administration of the colony stimulating factor-1 receptor (CSF1R) inhibitor PLX5622 (1,200 mg/kg chow) where younger, 3-week-old mice with a shorter, 3-day feed/withdrawal period were used for this depletion step. This was modeled on evidence that PLX5622 achieves comparably rapid depletion in juvenile mice. One study found >99% microglial depletion in the juvenile visual cortex within approximately 4 days of chow administration beginning at postnatal day 18 (Figueroa Velez et al., 2022). This rate was comparable to the ~3 days reported for near-complete depletion in adult mice (Spangenberg et al., 2019). After, the percentage of remaining endogenous microglia in the mice were recorded before a stereotaxic injection of the barcode-labeled microglia donor microglia was transplanted. The assessment of how successful the transplantation went will be assessed in the mouse model at approximately 30 days (~4 weeks) post-transplant, as that is when the exogenous microglia cells are expected to have proliferated and repopulated the depleted nich (Xu et al., 2020). This will be done via immunohistochemistry for GFP signaling.

2.1.4 Bone Marrow-Derived Macrophage Isolation Pilot

In parallel, a pilot test of bone marrow-derived macrophage (BMDM) isolation was performed using bone marrow harvested from the femur and tibia of an adult wild-type mouse, following standard BMDM isolation methodology where marrow is flushed from the femur and tibia, filtered to a single-cell suspension, and cultured in the presence of macrophage colony-stimulating factor (M-CSF), either as recombinant cytokine or via L929-cell-conditioned medium, which drives differentiation of bone marrow progenitors into adherent macrophages over approximately 6-7 days (Weischenfeldt & Porse, 2008). This pilot was intended only to confirm that viable bone marrow could be harvested and cultured from an adult donor as a

backup source for the microglia engraftment pipeline (Section 2.1.3), and differentiation success was not assessed by marker staining or a functional assay in this pilot round.

2.2 Aim 2: CHIP × AD Organoid Model

2.2.1 hESC Maintenance

The parental human embryonic stem cell (hESC) line, H9, is maintained under both feeder-dependent and feeder-free culture conditions. Cells are maintained on an approximately 6-day passage cycle, with routine medium changes performed throughout the maintenance period. Under feeder-dependent conditions, hESCs are maintained in DMEM/F12 supplemented with serum replacement (SR) on Mouse Embryonic Fibroblasts (MEF). In parallel, hESCs are maintained under feeder-free conditions using mTeSR medium (STEMCELL Technologies, n.d.), as the last step before hematopoietic differentiation.

For feeder-dependent cultures, hESCs are routinely passaged using a manual grid-based method, in which colonies are mechanically divided into smaller pieces using an insulin needle. The laboratory is also evaluating a gentle cell dissociation protocol as an alternative passaging method from StemCell Technologies (STEMCELL Technologies, n.d.).

For the CRISPRi screening workflow, an engineered H9 hESC line is maintained to stably express doxycycline-inducible dCas9 and mCherry (dCas9-mCh). This is maintained in parallel with the parental H9 line to serve as a control background. The dCas9-mCherry line was generated by a lentiviral transduction with the pAAVS1-NDi-CRISPRi construct (Mandeger et al., 2016). This engineered line essentially provides the CRISPRi machinery required for the subsequent gene-change experiments. It is important to note that AAVS1-integrated, doxycycline-inducible transgenes in hESC lines have been identified to cause some issues for iPSC-to-myeloid differentiation protocols as transgene silencing at this locus has been reported to occur in a promoter-dependent way during myeloid differentiation of hPSCs (Klatt et al., 2020). The specific TRE3G promoter used in TET-inducible constructs like this one have been shown to become methylated even in the undifferentiated iPSC stage as one study reported 95.3-98.2% methylation (Wang et al., 2025). Inducible transgenic systems in hPSCs have also been shown to face reduced inducibility following differentiation into macrophage and microglial lineages which is the workflow we planned to do (Gallagher et al., 2025). This raises the possibility that dCas9-mCh expression could be affected by the HPC or iMGL independent of CRISPR-CHIP mutations.

2.2.2 Generation of dCas9-mCh CHIP-Variant Lines

CHIP driver mutations (TET2, DNMT3A, ASXL1) are introduced into the dCas9-mCh hESC line using CRISPR-Cas9-mediated genome editing. These edits are delivered to the hESCs by electroporation after which cells are dissociated and plated into 24-well plates at limiting dilution to allow the isolation of individual clones. Candidate clones will be identified by morphological screening over ~1-2 weeks, followed by an expansion and genetic validation before using them in later experiments (Chadarevian et al., 2023). This general strategy of CRISPR editing of a parental hPSC line followed by clonal selection to generate a matched isogenic mutant/wild-type pair is the same approach used to generate the specific CHIP-variant iMGL lines (DNMT3A R882H/WT, TET2 DelE3-E11/WT, ASXL1 E635fs*15/WT) described in a closely related published isogenic model built on an APOE ε3/ε3 background (Huang et al., 2026).

2.2.3 HPC Differentiation and FACS Sorting

Following editing and clonal selection, feeder-free hESC lines (CHIP-variant and isogenic wild-type control) are differentiated into hematopoietic progenitor cells (HPCs). The resulting HPCs are then exposed to doxycycline (Dox) to induce expression of mCherry and dCas9. This Dox-inducible differentiation step occurs prior to FACS sorting, with Dox exposure initiated approximately 1-2 days before sorting. HPCs are then analyzed and sorted by fluorescence-activated cell sorting (FACS) using fluorescently conjugated antibodies against CD34 (CD34-FITC), CD43 (CD43-APC), and CD45 (CD45-APC/Cy7). mCherry fluorescence is additionally used to identify cells retaining the Cas9-mCherry construct, while DAPI is used as a viability dye to exclude dead cells from the sorted population. Because of the AAVS1/TRE3G silencing risk described in 2.2.2, mCherry and dCas9 expression are monitored at the HPC stage via this FACS panel and possibly at the iMGL stage as well to detect if there's any silencing of the gene construct.

2.2.4 Lentiviral gRNA Delivery Timing

Because mature, differentiated microglia are markedly resistant to lentiviral transduction relative to their progenitor stages, the timing of gRNA delivery relative to the iPSC to HPC to iMGL differentiation timeline is a key design parameter (Dolan et al., 2023). Dolan et al. developed a dedicated lentiviral transduction protocol for use directly on more mature iMGLs, which are otherwise resistant to standard lentiviral entry by co-delivering the lentivirus with SIV-derived Vpx packaged in virus-like particles (which degrade the restriction factor SAMHD1). This was seen to raise transduction efficiency from ~4% (lentivirus alone) to ~89%. In their protocol, transduction is performed at day 35 of the iMGL differentiation timeline, with downstream assays or experiments conducted at day 42 (7 days post-transduction), a recovery window chosen because transduction transiently increases expression of interferon-stimulated genes that decay back toward baseline by day 7 post-transduction, allowing iMGL morphology and transcriptional profile to normalize before use.

Because this project's hESC line already stably expresses Cas9 (fused to mCherry) prior to differentiation only the gRNA itself needed to be delivered by lentivirus, and this project follows the Dolan et al. timeline for that delivery.

2.2.5 iMGL Differentiation and Organoid Incorporation

HPCs are differentiated into induced microglia-like cells (iMGLs) using a cytokine cocktail including M-CSF, IL-34, and TGF-β1, mimicking the signaling niche microglial progenitors encounter during brain colonization in vivo (Buonfiglioli et al., 2025). iMGL incorporation into AD-model cerebral organoids follows the co-culture strategy established by Buonfiglioli et al., in which matched, isogenic HPCs rather than fully matured iMGLs are directly co-cultured with cerebral organoids, allowing microglial maturation to occur within the organoid microenvironment itself. This is reported to produce a more physiologically representative, better-integrated microglial population than introducing already-mature iMGLs into a pre-formed organoid, and has been used similarly in other recently published microglia-containing cerebral organoid systems that report physiologically representative microglial proportions (~7% CD45+/CD11b+/Iba1+ cells) using an analogous HPC/iPSC co-culture strategy (Osborn et al., 2025). Figure 1 showcases the entire protocol timeline for the Aim 2 project including the hESC maintenance, differentiation into HPCs, differentiation into iMGLs, and the co-culturing into organoids. It also includes important media change steps and the papers the protocols were sourced from.

Figure 1.

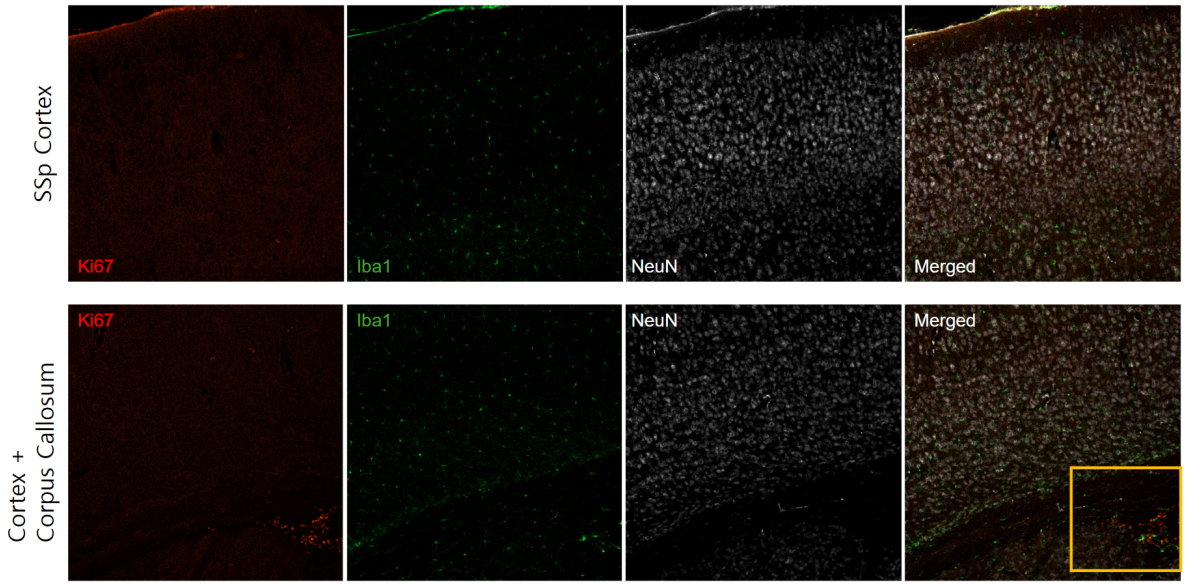
3. RESULTS

3.1 Aim 1: Cancer × AD In Vivo Model

3.1.1 Postnatal Electroporation and Immunohistochemistry Staining

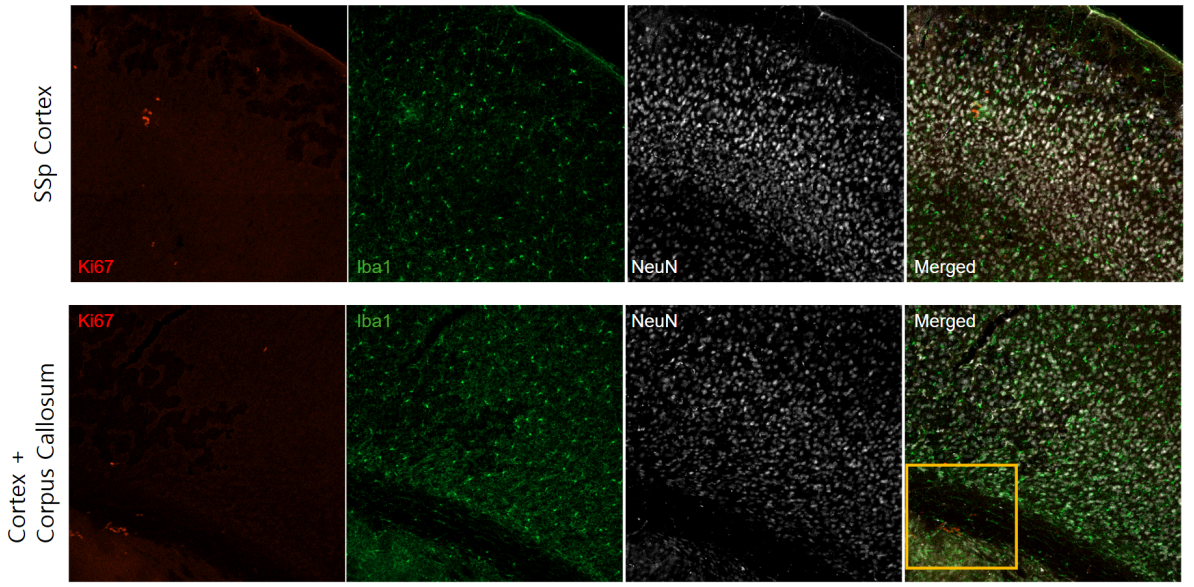
Figure 2.

IHC results – WT mouse, 10 weeks, male



The part marked with yellow box may indicate hint of precancerous growth, but we need reporter line to make sure it is precancerous cells mediated by vector delivery

IHC results – APP/PS1 mouse, 10 weeks, male



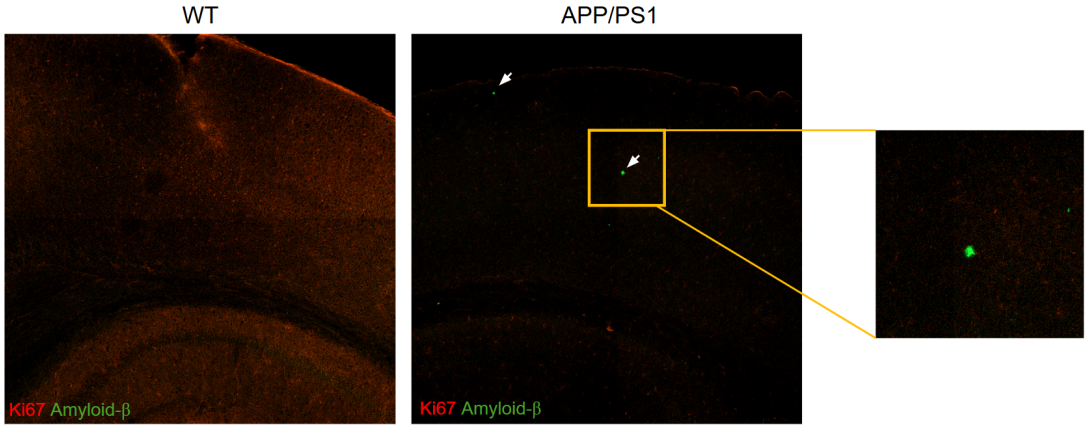
The part marked with yellow box may indicate hint of precancerous growth, but we need reporter line to make sure it is precancerous cells mediated by vector delivery

Data collected and organized by Seungyoon Yu

Immunohistochemical staining and slide scanning were completed for the 10-week electroporated cohort of WT and APP/PS1 male mice. Ki67 immunoreactivity was low with a majority of the somatosensory (SSp) cortex showing no detectable Ki67+ nuclei in either genotype. There was a discrete cluster of Ki67+ cells observed specifically at the cortex/corpus callosum boundary in the WT and APP/PS1 sections (yellow boxed regions). This pattern was

not detected anywhere else in the sampled tissue. Iba1+ microglia also seemed to be distributed evenly through the gray and white matter in both regions and genotypes. The morphology looks typical of microglia and there is no increased density or clustering around the Ki67+ regions. NeuN staining shows a normal, dense layer and neuronal pattern in the cortex for both genotypes, with no interruption in the cortical layering.

Figure 3.



At 10 weeks it is still early to see obvious Amyloid-beta plaques, but we were able to capture some of Amyloid-beta positive spots in cortices of APP/PS1 mice only (marked with arrows)

In a separate panel that is comparing Ki67 and amyloid-β staining between genotypes, no amyloid-β signal was detected in the WT cortex or hippocampus while there was small amyloid-β positive points detected in the APP/PS1 cortex (arrows). There was no comparable signal seen in the WT signal.

3.1.2 Primary Microglia Isolation and Barcoded Viral Labeling

Primary microglia isolated from wild-type donor cortical tissue were successfully cultured using the mixed glial culture/shake-off method, yielding 500,000 viable cells per flask for downstream viral labeling. Harvested microglia were plated on PLO-coated 6-wells at the density of 40,000 cells / cm^2.

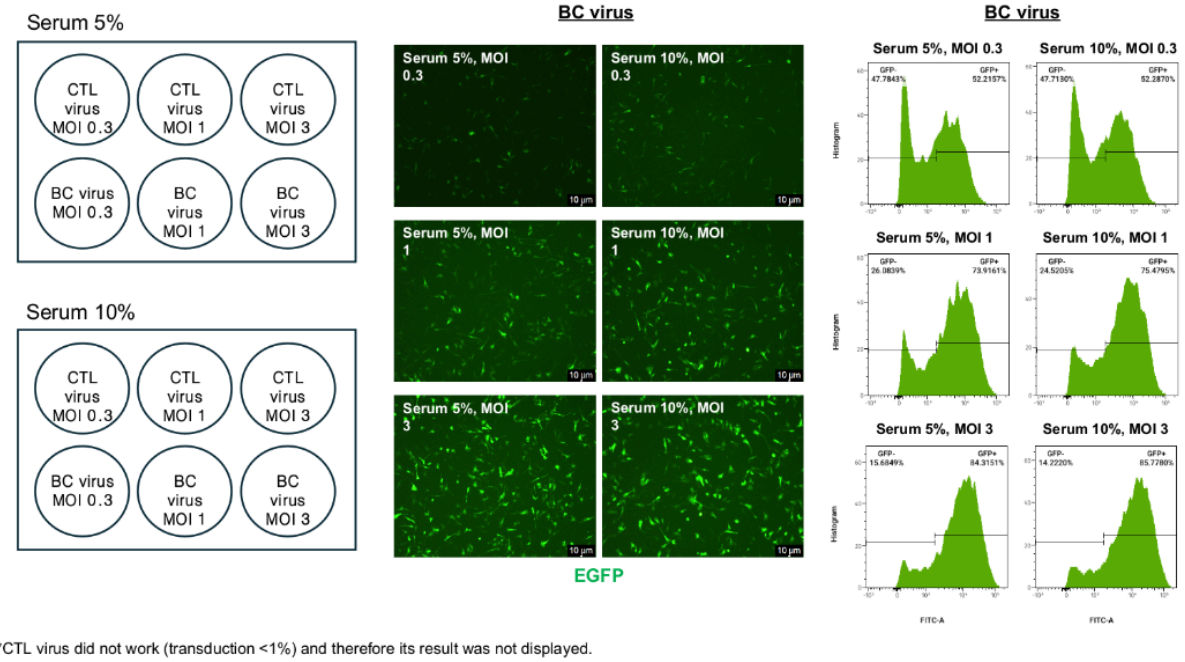
Table 3. Transduction efficiency of barcode lentivirus under different MOI and serum conditions.

Condition	Serum 5% (%GFP+)	Serum 10% (%GFP+)
MOI 0.3	52.2%	52.3%

MOI 1	73.9%	75.5%
MOI 3	84.3%	85.8%

Fluorescence microscopy supported these flow cytometry findings as the higher the MOI, the higher the density of EGFP+ cells. There seems to not be a qualitative difference between the two serum conditions as seen in Figure 4. below. The CTL lentivirus had a negligible transduction of <1% GFP across all the conditions tested so it was excluded from the quantitative comparison. This might be an issue with the preparation as a functional lentivirus shouldn't perform differently because of the cargo.

Figure 2.



*CTL virus did not work (transduction <1%) and therefore its result was not displayed.

Data collected and organized by Seungyoon Yu

3.1.3 Microglia Engraftment Pilot

Depletion in this pilot was incomplete but this is an outcome consistent with a well-documented pattern in the CSF1R-inhibitor literature where standard longer-duration PLX5622 timelines frequently only achieved partial (~65-80%) microglial depletion instead of seeing complete elimination. Usually any surviving microglia proliferated and repopulated the niche once the inhibitor was removed (Kodali et al., 2024). Transplantation still proceeded and engraftment outcomes are still pending.

3.1.4 Bone Marrow-Derived Macrophage Isolation Pilot

Bone marrow was successfully harvested and cultured from the femur and tibia of an adult wild-type mouse using standard BMDM isolation methodology (Section 2.1.4). Differentiation into mature macrophages was not done in this pilot as it is served to be a back-up if the primary microglia engraftment pilot did not work.

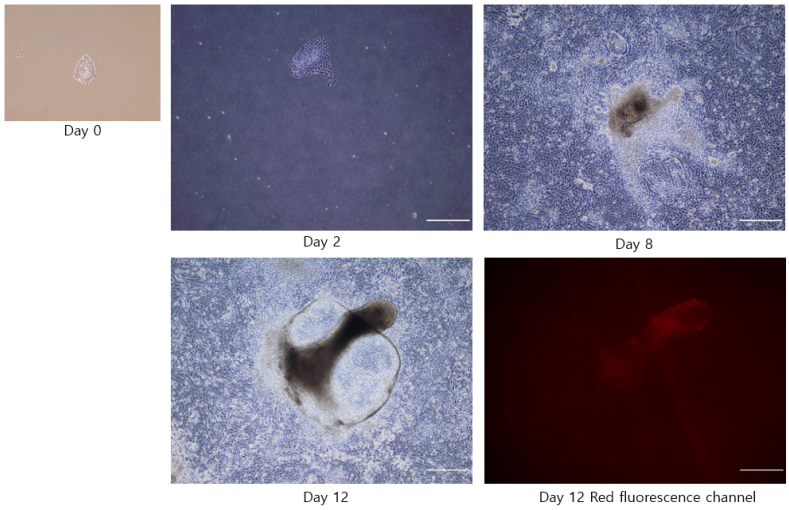
3.2 Aim 2: CHIP × AD Organoid Model

3.2.1 Generation of Isogenic CHIP-Variant Lines

Generation of the isogenic CHIP-variant lines is currently ongoing. Candidate edited hESC lines are being expanded and maintained prior to differentiation into hematopoietic progenitor cells and subsequent iMGL differentiation. Final characterization and validation of the CHIP-variant lines will be performed following completion of the differentiation workflow.

3.2.2 HPC Differentiation and FACS Sorting

Figure 3.



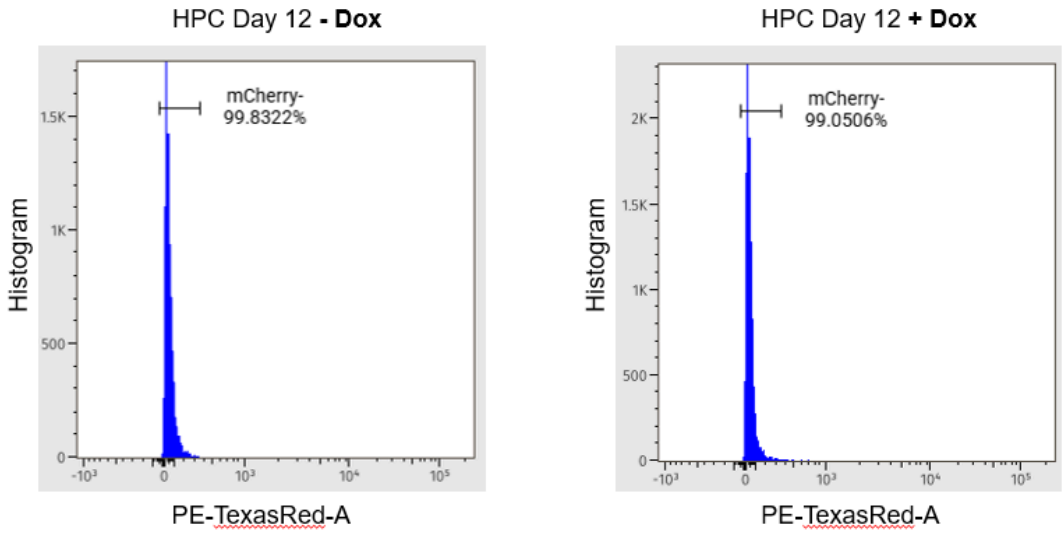
Images taken by Seungyoon Yu

Differentiation of the dCas9-mCh hESC line into hematopoietic progenitor cells followed the expected morphological progression across the embryoid-body-based protocol (Figure 3). On Day 0, small, compact colonies with irregular, spiked borders were observed. By Day 2, colonies had expanded into an adherent monolayer with a cobblestone-like cell morphology, consistent with early mesodermal/hemogenic induction. By Day 8, a confluent adherent monolayer had formed, within which a discrete, darker, pigmented focal cluster was visible which is consistent with the emergence of a hemogenic endothelium patch beginning to generate hematopoietic

cells. By Day 12, this cluster had developed into a distinct, floating, cystic structure with darker pigmented material, sitting atop the underlying adherent monolayer. The imaging of this same structure in the red fluorescence channel showed visible red signal localized specifically to it.

Despite this visible red signal on fluorescence microscopy, quantitative flow cytometry of the bulk Day 12 HPC population did not align with this finding. mCherry positivity was assessed in matched −doxycycline (−Dox) and +doxycycline (+Dox) conditions, with Dox added 1-2 days prior to sorting to induce dCas9-mCherry expression. The two conditions were nearly indistinguishable with 99.83% of cells expressing mCherry-negative in the −Dox condition, versus 99.05% mCherry-negative in the +Dox condition, a difference of under one percentage point (Figure 4). In other words, doxycycline induction seemed to produce no substantial increase in the mCherry+ fraction of the bulk HPC population at this stage although a difference was expected since Dox includes the expression of mCherry and Cas9.

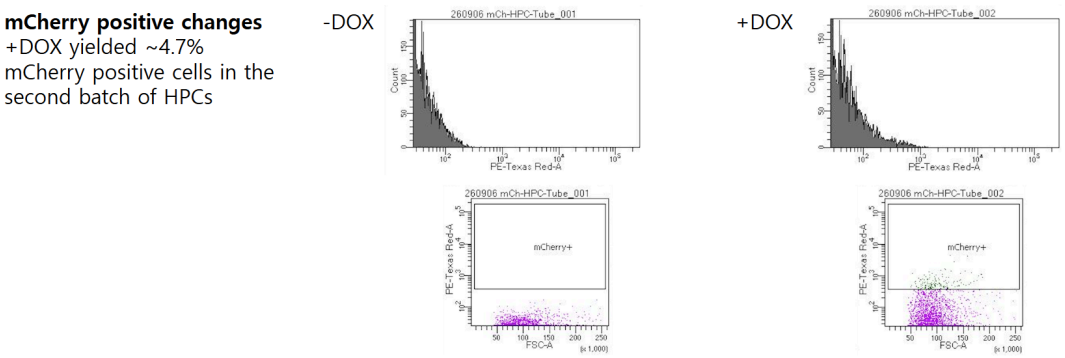
Figure 4.



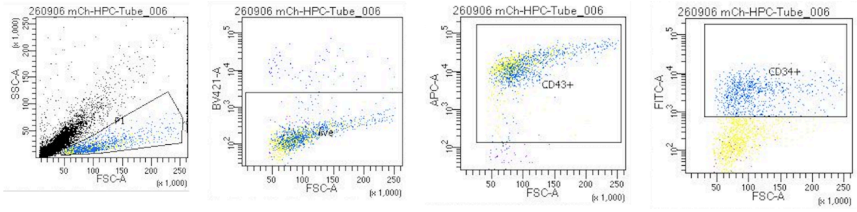
Data organized by Seungyoon Yu

A second batch of HPCs was later differentiated and assessed by FACS to determine whether the absent-Dox-induced mCherry signal observed in the first bath would replicate. In this second batch, +Dox induction yielded 4.7% mCherry-positive cells, compared to a -Dox histogram which showed no discernible positive population (Figure 5). Overall live-cell yield was low (<20% of the total cell suspension), but CD43 positivity, the primary hematopoietic progenitor marker, exceeded 90% among the live cells. There was also a clear CD34+ subpopulation present (Figure 5).

Figure 5.

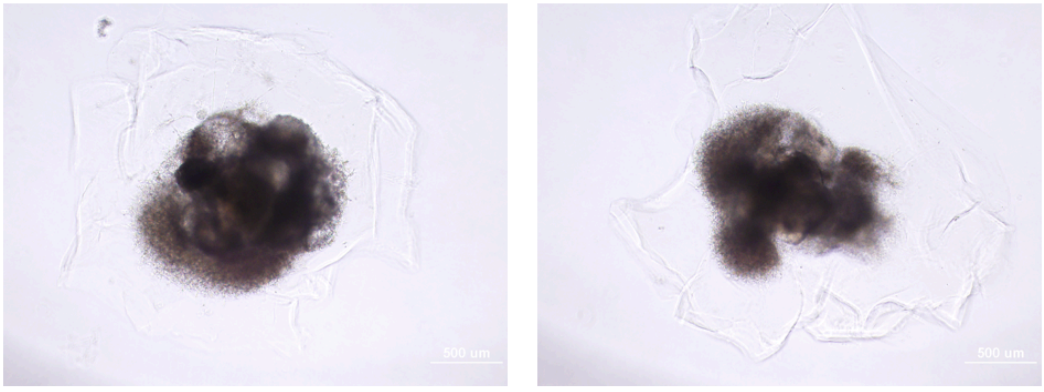


Overall yield for live cells were <20% of cells in suspension, but CD43+ rate was >90% for live cells



3.2.3 iMGL Differentiation and Organoid Incorporation

Figure 5.

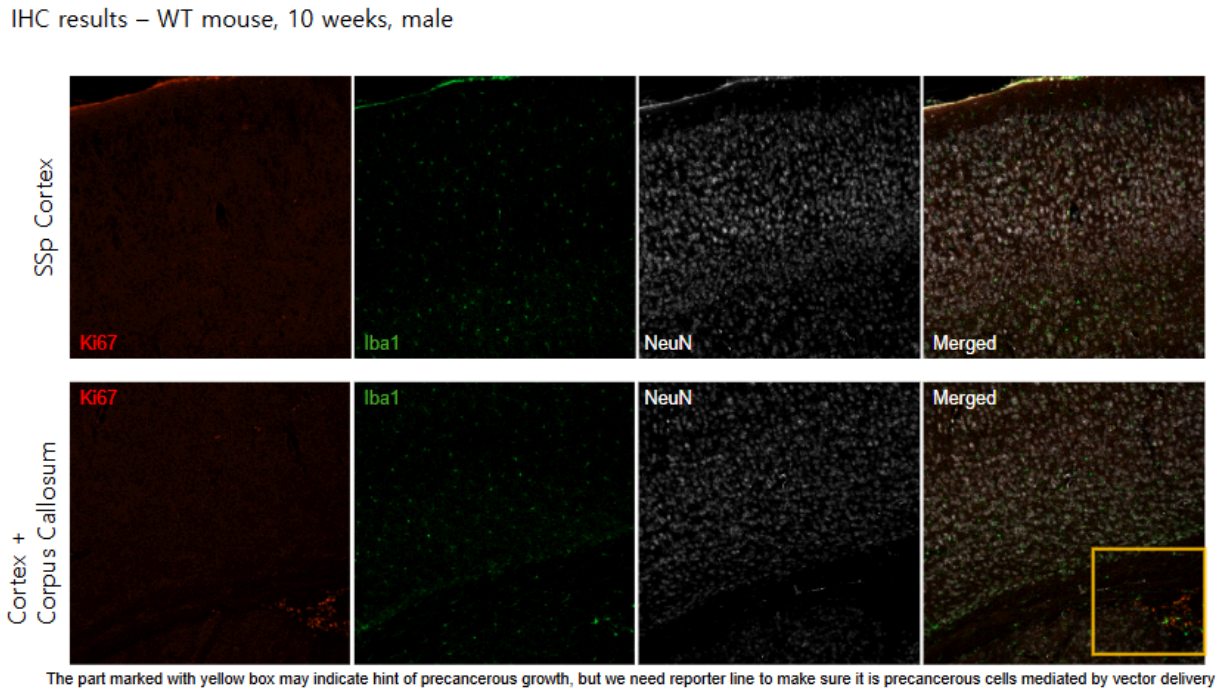


Organoids at Day 14

Images taken by Seungyoon Yu

Cerebral organoids were imaged at Day 14. At this stage, organoids appeared as compact, darkly opaque, lobulated spheroids approximately 500 µm in diameter. They are surrounded by a thin, translucent halo of loosely adherent material (Figure 5). This morphology is consistent with an early-stage cerebral organoid before the extended neuroepithelial expansion that is expected later

in culture, and is well before the ~40-day maturation window at which HPC co-culture is introduced in this protocol (Section 2.2.5).



4. DISCUSSION

4.1 Aim 1: Cancer × AD In Vivo Model

4.1.1 Postnatal Electroporation and Proliferation Staining

The Ki67+ cell cluster observed specifically at the cortex/corpus callosum boundary in both genotypes (Section 3.1.1) is a notable preliminary finding. The corpus callosum is a known migratory route for subventricular zone (SVZ)-derived neural stem/progenitor cells. This was the population that was directly targeted by the postnatal electroporation in this protocol (Section 2.1.1). Diffuse gliomas arising from SVZ progenitors are well documented to invade and spread along white matter tracts, including the corpus callosum (Sinnaeve et al., 2017). The spatial localization of this proliferative signal is consistent with electroporated progenitor-derived cells that have migrated along this expected anatomical route. This is an associative conclusion though because the present pilot construct lacks a lineage-specific reporter so it is not possible to confirm if these Ki67+ cells actually derive from the construct-expressing cells or other proliferative populations that occupy near the corpus callosum. For example they could be ongoing adult SVZ neurogenesis, oligodendrocyte progenitor turnover, or ependymal cells dividing. Incorporating a fluorescent lineage reporter in future cohorts could fill in this gap.

It is also important to note that the Ki67+ pattern was seen in comparable size and location for both WT and APP/PS1 tissue which indicates that at 10 weeks, the amyloid genotype does not appear to modify the proliferative signal. This was anticipated as amyloid-β pathology is only now just seen to become detectable at this point and would not be expected to meaningfully influence a co-occurring proliferative phenotype yet (Figure 3). Iba1 and NeuN staining qualitatively did not have any standout findings as they were comparable across genotypes and regions which suggests that neither microglial activation or neuronal loss has developed by this timepoint which is consistent with the ~20-week tumor timeline established for the full model (Section 2.1.2) and the ~6-month amyloid plaque timeline that is typical of APP/PS1 mice.

The detection of the small region of amyloid-β reactivity in the APP/PS1 cortex, and being absent in the WT tissue can be used as a control as it confirms that the staining protocol is genotype-specific and is sensitive enough to detect amyloid accumulation at a very early, pre-plaque stage, even though the mature compact plaques haven't formed yet. This 10-week pilot dataset proves that both proliferation and amyloid pathology are able to be detected but there need to be longer cohorts to actually see the interaction between GBM and AD.

4.1.2 Barcoded Viral Labeling Pilot

The transduction optimization panel established that labeling efficiency of donor microglia with the BC lentivirus is governed almost entirely by MOI rather than serum concentration, with efficiency rising from ~52% at MOI 0.3 to ~85% at MOI 3 regardless of the serum condition. Because the barcode's usefulness for clonal tracking depends on most labeled cells carrying a single integration event, the ideal labeling condition is not simply "the highest transduction efficiency achievable," but the highest efficiency that still falls within the range where single-integration events are dominant (Section 2.1.3). This led to an MOI of 0.3 to be selected for further experiments. Despite producing the lowest overall labeling efficiency (~52%), at this lower MOI, the majority of cells that become transduced are expected to receive a single lentiviral particle, minimizing multiple integration events and preserving the ability to associate an individual barcode with a specific donor cell lineage. The higher labeling efficiencies observed at MOI 1 and 3 would increase the number of labeled cells but would also increase the likelihood of multiple integrations per cell, reducing the interpretability of barcode-based clonal tracking.

The negligible transduction observed with the non-barcoded control (CTL) lentivirus (<1% GFP+ across all conditions) may be a technical problem as this control uses the same lentiviral packaging backbone as the BC virus. This large discrepancy is more consistent with a technical issue and will be re-validated when another trial run can be completed.

4.1.3 Microglia Engraftment Pilot

The PLX5622 depletion pilot achieved only partial clearance of endogenous microglia rather than the near-complete depletion that is generally used to maximize the engraftment of transplanted donor cells (Section 2.1.3). This result is consistent with the broader CSF1R-inhibitor literature, in which PLX5622 treatment can leave a residual endogenous microglial population, and surviving cells can rapidly repopulate the niche following inhibitor withdrawal (Kodali et al., 2025). The incomplete depletion represents a potential limitation of the present engraftment protocol, because residual host microglia may occupy the available niche before or during donor-cell engraftment. But, because donor microglia were transplanted despite the incomplete depletion and engraftment outcomes are still pending, the extent to which niche availability affected donor-cell engraftment cannot yet be determined. Once the brain sections are analyzed, the observed percentage of GFP+ donor cells should be considered alongside the depletion efficiency to determine whether incomplete host-cell clearance is a likely contributor to the final engraftment outcome.

Several published strategies suggest potential approaches for improving endogenous microglial depletion in future iterations of the engraftment protocol. One option would be to extend the duration of PLX5622 treatment. Xu et al., for example, used a 2-week PLX5622 regimen together with irradiation preconditioning and achieved greater than 99% depletion prior to donor-cell transplantation (Xu et al., 2020). Compared with the 3-day feeding scheme used in the present pilot, this may suggest that the short treatment window may have been insufficient to achieve the degree of niche clearance required for efficient donor engraftment. It is important to note that irradiation may be undesirable for the present model because the eventual host animals will combine amyloid pathology with an electroporation-induced oncogenic manipulation which might be potentially limited by the physiological tolerance of the mouse.

A potentially more compatible alternative is a cyclic CSF1R-inhibitor strategy. Chen et al. demonstrated that three cycles of PLX3397 (a CSF1R inhibitor related to PLX5622 but not the same compound), created a therapeutic window that permitted substantial donor microglia replacement without irradiation or chemotherapy preconditioning. Importantly, this approach was validated in both a lysosomal storage disease model and an AD model (Chen et al., 2025). These findings suggest that repeated depletion cycles may provide a way to create sufficient niche availability while avoiding the harsher conditioning approaches used in some transplantation protocols. For the present system, a cyclic depletion strategy may therefore represent a particularly promising future direction, especially once donor engraftment is evaluated in the context of the combined GBM/AD model.

4.1.4 Bone Marrow-Derived Macrophage Isolation Pilot

Bone marrow was successfully harvested and cultured from an adult wild-type donor, confirming feasibility of this backup cell source for the microglia engraftment pipeline. Because differentiation into mature macrophages was not yet confirmed by marker staining in this pilot, this remains an open next step before BMDMs can be considered a validated backup population. This would be a comparatively low-cost addition to the next round of experiments and would provide an alternative to the engraftment pipeline.

4.2 Aim 2: CHIP × AD Organoid Model

4.2.1 Generation of Isogenic CHIP-Variant Lines

Results are still a work in progress.

4.2.2 HPC Differentiation and FACS Sorting

The Day 12 FACS results provide direct, quantitative evidence consistent with the AAVS1/TRE3G silencing risk raised in Methods (Section 2.2.1) as doxycycline induction produced almost no change in the mCherry+ fraction of the bulk HPC population (99.83% mCherry-negative without Dox vs. 99.05% mCherry-negative with Dox. Given that the same TRE3G promoter driving this construct has been reported to reach 95-98% methylation as early as the undifferentiated iPSC stage (Wang et al., 2025), and that inducible transgenic systems in hPSCs have been specifically shown to lose inducibility following myeloid/microglial differentiation (Gallagher et al., 2025), a possible explanation for this result is that the dCas9-mCherry cassette has already become substantially silenced by the HPC stage, well before iMGL differentiation or CRISPRi-based phenotyping would occur. This is a meaningful concern for the project's overall design as if dCas9 itself is silenced by this stage, later CRISPRi knockdown of CHIP-relevant genes may fail regardless of which gRNAs are used, and any resulting "no phenotype" observation in downstream experiments would be uninterpretable without first ruling out this possibility.

The mCherry induction that was observed in this second HPC batch (~4.7% +Dox vs negligible -Dox) contradicts the “fully silenced” hypothesis introduced in the previous paragraph. Instead of a complete, uniform silencing of the AAVS1-construct, this result is more consistent a small subset of cells retaining inducible expression while the majority are resistant to Dox. This is supported by the promoter-methylation mechanism described by Wang et al. and Klatt et al. where methylation does not need to be complete or uniform across every cell in a population. Batch-to-batch variability in induction efficiency (near-0% vs. ~4.7%) may reflect differences in passage number, differentiation efficiency, or the degree of methylation that accumulated prior to the Dox exposure and it is worth it to track more differentiation runs.

An interesting finding from this second run was the strong CD43+ (>90%) and CD34+ positivity in this batch as it indicates that the hematopoietic progenitor identity itself is being achieved efficiently. Even though ~4.7% induction is far below what is needed for the CRISPRi-based phenotyping, across a bulk population, this just proves that dCas9 functionality should be directly tested for a well-characterized control gene before moving on to the CHIP-variant lines. The low overall cell yield (<20%) is also worth looking into as poor viability could be contributing to the inconsistent induction results across batches.

One inconsistency with this though is that fluorescence microscopy of the Day 12 culture showed a visible red signal localized to the same structure that appeared as a dark, pigmented focus in brightfield imaging from Day 8 onward (Section 3.2.2), which could be read as evidence against silencing. However, this pigmented appearance is also consistent with a well-known feature of hematopoietic differentiation protocols that is unrelated to any fluorescent reporter as primitive erythroid cells generated during this differentiation stage become hemoglobinized and can appear reddish-brown by brightfield microscopy and may also generate non-specific signal in red fluorescence channels. Given that the quantitative flow cytometry data, that is run on dissociated single cells, showed no meaningful mCherry induction, the fluorescence microscopy image should not be taken as confirmation that the construct remains active.

4.2.3 iMGL Differentiation and Organoid Incorporation

Organoids imaged at Day 14 showed compact, darkly opaque, lobulated spheroid morphology approximately 500 μm in diameter, consistent with early-stage cerebral organoids prior to extended neuroepithelial expansion. This stage remains well before the ~40-day maturation window at which HPC co-culture is introduced under the Buonfiglioli et al. protocol, so organoid morphology at this early timepoint is not yet informative about eventual microglial incorporation success. Right now, it primarily serves as a checkpoint that organoid formation and gross morphology are proceeding on the expected developmental timeline before the more consequential co-culture step is reached. Given the HPC-stage silencing concern raised above (Section 4.2.2), it is important to re-verify mCherry/dCas9 expression again at the point of organoid incorporation.

4.3 Cross-Cutting Limitations and Future Directions

Several limitations span both workflows this summer. First, both the in vivo (Aim 1) and in vitro (Aim 2) pipelines are still largely in a foundational, protocol-establishment phase. Second, the two most concrete pilot findings from this summer, the incomplete PLX5622 depletion (Section 4.1.3) and the near-complete absence of Dox-induced mCherry expression at the HPC stage (Section 4.2.2), point to the same broader problem that technical and epigenetic constraints specific to the myeloid/microglial lineage repeatedly complicate experiments that behave more

predictably in other cell types or contexts, explaining why the literature review underlying both aims (Section 1.6) emphasized functional, multi-checkpoint validation over reliance on any single marker or readout. The apparent AAVS1/TRE3G silencing observed in Aim 2 is a the most urgent limitation to resolve, since it might impact the interpretability of the CRISPRi-based phenotyping. Without confirming that dCas9 remains active in cells actually used for phenotyping, a lack of observed CHIP-variant phenotype cannot be distinguished from a failure of the editing machinery itself. Future work should prioritize resolving these two specific technical constraints before the isogenic gene-perturbation phenotyping central to both aims can be meaningfully interpreted.

5. CONCLUSION

To conclude, this summer's work across both aims was foundational and proposed two distinct genetic routes into the same underlying biological question: what pushes microglia from a helpful, homeostatic state toward a harmful, disease-associated one in Alzheimer's disease. Both the cancer-AD and CHIP-AD literature point to this question as a genuine gap in the field as both topics have so far been addressed almost entirely through correlational human and mouse data. By using controlled, isogenic workflows, in vivo models, and an in vitro isogenic organoid system these projects hope to generate causal data that the field lacks to explain Alzheimer’s complex relationship with cancer and with CHIP. By doing so the field can also understand microglia’s behavior in these pathologies. The technical obstacles encountered this summer like incomplete microglial depletion, and a likely silencing issue in the inducible CRISPR machinery are problems that will be solved before that causal test can be run, and identifying them clearly, with a literature-grounded explanation and a concrete path forward for each, are the next steps for this project. The lab also plans to finish the current pilot for the co-organoid model. With these pipelines now established and their key failure points understood, the next phase of this work is positioned to generate the first direct, mechanistic evidence connecting these two AD risk factors to the specific microglial states identified in Section 1.4.

Works Cited

Addgene: pAAVS1-NDi-CRISPRi (Gen1). (n.d.). https://www.addgene.org/73497/

Albanese, E., Launer, L. J., Egger, M., Prince, M. J., Giannakopoulos, P., Wolters, F. J., & Egan, K. (2017). Body mass index in midlife and dementia: Systematic review and meta‐regression analysis of 589,649 men and women followed in longitudinal studies. *Alzheimer S & Dementia Diagnosis Assessment & Disease Monitoring*, *8*(1), 165–178. https://doi.org/10.1016/j.dadm.2017.05.007

Amann, L., & Prinz, M. (2026). Gateways for myeloid cell entry into the central nervous system. *Neuron*, *114*(14), 2505–2520. https://doi.org/10.1016/j.neuron.2026.04.001

Ardura-Fabregat, A., Bosch, L. F. P., Wogram, E., Mossad, O., Sankowski, R., Aktories, P., Kieger, L., Cook, J., Hasavci, D., Ulupinar, H., Brock, D., Wang, F., Iovino, N., Wald, S., Preissl, S., Yilmaz, B., Schnepf, D., Macpherson, A. J., Blank, T., . . . Prinz, M. (2025). Response of spatially defined microglia states with distinct chromatin accessibility in a mouse model of Alzheimer's disease. *Nature Neuroscience*, *28*(8), 1688–1703. https://doi.org/10.1038/s41593-025-02006-0

Benbenishty, A., Gadrich, M., Cottarelli, A., Lubart, A., Kain, D., Amer, M., Shaashua, L., Glasner, A., Erez, N., Agalliu, D., Mayo, L., Ben-Eliyahu, S., & Blinder, P. (2019). Prophylactic TLR9 stimulation reduces brain metastasis through microglia activation. *PLoS Biology*, *17*(3), e2006859. https://doi.org/10.1371/journal.pbio.2006859

Bouzid, H., Belk, J. A., Jan, M., Qi, Y., Sarnowski, C., Wirth, S., Ma, L., Chrostek, M. R., Ahmad, H., Nachun, D., Yao, W., Bis, J., Psaty, B., Beiser, A., Bick, A. G., Bis, J. C., Fornage, M., Longstreth, W. T., Lopez, O. L., . . . Jaiswal, S. (2023). Clonal hematopoiesis is associated with protection from Alzheimer's disease. *Nature Medicine*, *29*(7), 1662–1670. https://doi.org/10.1038/s41591-023-02397-2

Buonfiglioli, A., Kübler, R., Missall, R., De Jong, R., Chan, S., Haage, V., Wendt, S., Lin, A. J., Mattei, D., Graziani, M., Latour, B., Gigase, F., Nygaard, H. B., De Jager, P. L., & De Witte, L. D. (2024). A microglia-containing cerebral organoid model to study early life immune challenges. *bioRxiv (Cold Spring Harbor Laboratory)*. https://doi.org/10.1101/2024.05.24.595814

Cellecta. (n.d.). *CloneTracker™ Barcode Libraries and Kits*. Cellecta. https://cellecta.com/collections/clonetracker-barcode-libraries-and-kits

Chadarevian, J. P., Davtyan, H., Lombroso, S. I., Bennett, F. C., & Blurton-Jones, M. (2023a). CRISPR generation of CSF1R-G795A human microglia for robust microglia replacement in a chimeric mouse model. *STAR Protocols*, *4*(3), 102490. https://doi.org/10.1016/j.xpro.2023.102490

Chadarevian, J. P., Davtyan, H., Lombroso, S. I., Bennett, F. C., & Blurton-Jones, M. (2023b). CRISPR generation of CSF1R-G795A human microglia for robust microglia replacement in a chimeric mouse model. *STAR Protocols*, *4*(3), 102490. https://doi.org/10.1016/j.xpro.2023.102490

Clements, M., Ragdale, H. S., Garcia-Diaz, C., & Parrinello, S. (2024). Generation of immunocompetent somatic glioblastoma mouse models through in situ transformation of subventricular zone neural stem cells. *STAR Protocols*, *5*(1), 102928. https://doi.org/10.1016/j.xpro.2024.102928

Dan, L., & Kang-Zheng, L. (2025). Optimizing viral transduction in immune cell therapy manufacturing: key process design considerations. *Journal of Translational Medicine*, *23*(1), 501. https://doi.org/10.1186/s12967-025-06524-0

De Bruijn, R. F., Bos, M. J., Portegies, M. L., Hofman, A., Franco, O. H., Koudstaal, P. J., & Ikram, M. A. (2015). The potential for prevention of dementia across two decades: the prospective, population-based Rotterdam Study. *BMC Medicine*, *13*(1), 132. https://doi.org/10.1186/s12916-015-0377-5

Dolan, M., Therrien, M., Jereb, S., Kamath, T., Gazestani, V., Atkeson, T., Marsh, S. E., Goeva, A., Lojek, N. M., Murphy, S., White, C. M., Joung, J., Liu, B., Limone, F., Eggan, K., Hacohen, N., Bernstein, B. E., Glass, C. K., Leinonen, V., . . . Stevens, B. (2023a). Exposure of iPSC-derived human microglia to brain substrates enables the generation and manipulation of diverse transcriptional states in vitro. *Nature Immunology*, *24*(8), 1382–1390. https://doi.org/10.1038/s41590-023-01558-2

Dolan, M., Therrien, M., Jereb, S., Kamath, T., Gazestani, V., Atkeson, T., Marsh, S. E., Goeva, A., Lojek, N. M., Murphy, S., White, C. M., Joung, J., Liu, B., Limone, F., Eggan, K., Hacohen, N., Bernstein, B. E., Glass, C. K., Leinonen, V., . . . Stevens, B. (2023b). Exposure of iPSC-derived human microglia to brain substrates enables the generation and manipulation of diverse transcriptional states in vitro. *Nature Immunology*, *24*(8), 1382–1390. https://doi.org/10.1038/s41590-023-01558-2

Dong, H., Sun, Y., Nie, L., Cui, A., Zhao, P., Leung, W. K., & Wang, Q. (2024). Metabolic memory: mechanisms and diseases. *Signal Transduction and Targeted Therapy*, *9*(1), 38. https://doi.org/10.1038/s41392-024-01755-x

Fernández, M. E., Croce, S., Boutin, C., Cremer, H., & Raineteau, O. (2011). Targeted electroporation of defined lateral ventricular walls: a novel and rapid method to study fate specification during postnatal forebrain neurogenesis. *Neural Development*, *6*(1), 13. https://doi.org/10.1186/1749-8104-6-13

Fitzpatrick, A. L., Kuller, L. H., Lopez, O. L., Diehr, P., O'Meara, E. S., Longstreth, W. T., & Luchsinger, J. A. (2009). Midlife and Late-Life Obesity and the risk of dementia. *Archives of Neurology*, *66*(3), 336–342. https://doi.org/10.1001/archneurol.2008.582

Gentle cell dissociation reagent for human ES/IPS cells | STEMCELL Technologies. (n.d.). https://www.stemcell.com/products/gentle-cell-dissociation-reagent.html

Grubman, A., Choo, X. Y., Chew, G., Ouyang, J. F., Sun, G., Croft, N. P., Rossello, F. J., Simmons, R., Buckberry, S., Landin, D. V., Pflueger, J., Vandekolk, T. H., Abay, Z., Zhou, Y., Liu, X., Chen, J., Larcombe, M., Haynes, J. M., McLean, C., . . . Polo, J. M. (2021). Transcriptional signature in microglia associated with Aβ plaque phagocytosis. *Nature Communications*, *12*(1), 3015. https://doi.org/10.1038/s41467-021-23111-1

Heneka, M. T., Van Der Flier, W. M., Jessen, F., Hoozemanns, J., Thal, D. R., Boche, D., Brosseron, F., Teunissen, C., Zetterberg, H., Jacobs, A. H., Edison, P., Ramirez, A., Cruchaga, C., Lambert, J., Laza, A. R., Sanchez-Mut, J. V., Fischer, A., Castro-Gomez, S., Stein, T. D., . . . Riechers, S. (2024). Neuroinflammation in Alzheimer disease. *Nature Reviews. Immunology*, *25*(5), 321–352. https://doi.org/10.1038/s41577-024-01104-7

Hinte, L. C., Castellano-Castillo, D., Ghosh, A., Melrose, K., Gasser, E., Noé, F., Massier, L., Dong, H., Sun, W., Hoffmann, A., Wolfrum, C., Rydén, M., Mejhert, N., Blüher, M., & Von Meyenn, F. (2024). Adipose tissue retains an epigenetic memory of obesity after weight loss. *Nature*, *636*(8042), 457–465. https://doi.org/10.1038/s41586-024-08165-7

Huang, A. Y., Zhou, Z., Talukdar, M., Enyenihi, L., Miller, M. B., Chhouk, B., Rosen, I., Zheng, M., Zhou, M., Yang, A., Stronge, E., Durens, M., Nguyen, M., Choi, J., Zhao, B., Khoshkhoo, S., Kim, J., Andersen, R., An, Z., . . . Walsh, C. A. (2026). Somatic cancer variants enriched in Alzheimer's disease microglia-like cells drive inflammatory and proliferative states. *Cell*, *189*(12), 3719-3735.e24. https://doi.org/10.1016/j.cell.2026.03.040

Jaiswal, S., & Libby, P. (2019). Clonal haematopoiesis: connecting ageing and inflammation in cardiovascular disease. *Nature Reviews Cardiology*, *17*(3), 137–144. https://doi.org/10.1038/s41569-019-0247-5

Kessler, M. D., Damask, A., O'Keeffe, S., Banerjee, N., Li, D., Watanabe, K., Marketta, A., Van Meter, M., Semrau, S., Horowitz, J., Tang, J., Kosmicki, J. A., Rajagopal, V. M., Zou, Y., Houvras, Y., Ghosh, A., Gillies, C., Mbatchou, J., White, R. R., . . . Jorgenson, E. (2022). Common and rare variant associations with clonal haematopoiesis phenotypes. *Nature*, *612*(7939), 301–309. https://doi.org/10.1038/s41586-022-05448-9

Kim, H. J., Kim, K. W., Cha, D. H., Yoo, J., Kim, E. H., Chang, J. H., Kang, S., Park, J. W., Kim, J. H., Lee, Y., Lim, E., Kim, Y., Kim, M. H., Li, X., Lee, J. H., & Lee, J. H. (2025). Precancerous cells initiate glioblastoma evolution and contribute to intratumoral heterogeneity. *Cancer Discovery*, *15*(7), 1377–1391. https://doi.org/10.1158/2159-8290.cd-24-0234

Kodali, M., Madhu, L. N., Somayaji, Y., Attaluri, S., Huard, C., Panda, P. K., Shankar, G., Rao, S., Shuai, B., Gonzalez, J. J., Oake, C., Hering, C., Babu, R. S., Kotian, S., & Shetty, A. K. (2024). Residual microglia following short‐term PLX5622 treatment in 5xFAD mice

exhibit diminished NLRP3 inflammasome and mTOR signaling, and enhanced autophagy. *Aging Cell*, *24*(2), e14398. https://doi.org/10.1111/acel.14398

Kruman, I. I., Wersto, R. P., Cardozo-Pelaez, F., Smilenov, L., Chan, S. L., Chrest, F. J., Emokpae, R., Gorospe, M., & Mattson, M. P. (2004). Cell cycle activation linked to neuronal cell death initiated by DNA damage. *Neuron*, *41*(4), 549–561. https://doi.org/10.1016/s0896-6273(04)00017-0

Li, J., Joshi, P., Ang, T. F. A., Liu, C., Auerbach, S., Devine, S., & Au, R. (2021). Mid- to Late-Life body Mass Index and Dementia Risk: 38 years of Follow-up of the Framingham Study. *American Journal of Epidemiology*, *190*(12), 2503–2510. https://doi.org/10.1093/aje/kwab096

Li, J., Liu, C., Hu, X., Cai, Y., Ma, C., Luo, X., & Yan, X. (2014). Inverse correlation between Alzheimer's disease and cancer: implication for a strong impact of regenerative propensity on neurodegeneration? *BMC Neurology*, *14*(1), 211. https://doi.org/10.1186/s12883-014-0211-2

Lu, A., Chen, W., Dalby, M., Garcia, D. S., Vanheusden, M., De Vries, L. E., Van Lieshout, V., Martirosyan, A., Craessaerts, K., Moonen, S., Zielonka, M., Chrysidou, I., Misbaer, A., Wolfs, L., Pavie, B., Swaab, D., Thal, D. R., Huitinga, I., Rozemuller, A., . . . De Strooper, B. (2026). Human microglial transitions at the Aβ–tau inflection point associate with divergent pathways to dementia and resilience. *Nature Medicine*, *32*(6), 2047–2059. https://doi.org/10.1038/s41591-026-04393-8

Maes, M. E., Colombo, G., Schulz, R., & Siegert, S. (2019). Targeting microglia with lentivirus and AAV: Recent advances and remaining challenges. *Neuroscience Letters*, *707*, 134310. https://doi.org/10.1016/j.neulet.2019.134310

Majd, S., Power, J., & Majd, Z. (2019). Alzheimer's disease and Cancer: When two monsters cannot be together. *Frontiers in Neuroscience*, *13*, 155. https://doi.org/10.3389/fnins.2019.00155

Masuda, T., Sankowski, R., Staszewski, O., & Prinz, M. (2020). Microglia heterogeneity in the Single-Cell era. *Cell Reports*, *30*(5), 1271–1281. https://doi.org/10.1016/j.celrep.2020.01.010

Mercadante, A. A., & Kasi, A. (2023, August 14). *Genetics, Cancer Cell Cycle Phases*. StatPearls - NCBI Bookshelf. https://www.ncbi.nlm.nih.gov/books/NBK563158/

Ni, M., & Aschner, M. (2010). Neonatal Rat Primary Microglia: Isolation, Culturing, and Selected Applications. *Current Protocols in Toxicology*, *43*(1), Unit 12.17. https://doi.org/10.1002/0471140856.tx1217s43

Protocol for Culturing Rat Microglia: R&D Systems. (n.d.). R&D Systems. https://www.rndsystems.com/resources/protocols/protocol-culturing-rat-microglia

Ronan, L., Alexander-Bloch, A. F., Wagstyl, K., Farooqi, S., Brayne, C., Tyler, L. K., & Fletcher, P. C. (2016). Obesity associated with increased brain age from midlife. *Neurobiology of Aging*, *47*, 63–70. https://doi.org/10.1016/j.neurobiolaging.2016.07.010

Sinnaeve, J., Mobley, B. C., & Ihrie, R. A. (2017). Space invaders. American Journal of Pathology, 188(1), 29–38. https://doi.org/10.1016/j.ajpath.2017.08.029

Spangenberg, E., Severson, P. L., Hohsfield, L. A., Crapser, J., Zhang, J., Burton, E. A., Zhang, Y., Spevak, W., Lin, J., Phan, N. Y., Habets, G., Rymar, A., Tsang, G., Walters, J., Nespi, M., Singh, P., Broome, S., Ibrahim, P., Zhang, C., . . . Green, K. N. (2019). Sustained microglial depletion with CSF1R inhibitor impairs parenchymal plaque development in an Alzheimer's disease model. *Nature Communications*, *10*(1), 3758. https://doi.org/10.1038/s41467-019-11674-z

Steensma, D. P., Bejar, R., Jaiswal, S., Lindsley, R. C., Sekeres, M. A., Hasserjian, R. P., & Ebert, B. L. (2015). Clonal hematopoiesis of indeterminate potential and its distinction from myelodysplastic syndromes. *Blood*, *126*(1), 9–16. https://doi.org/10.1182/blood-2015-03-631747

Sun, N., Victor, M. B., Park, Y. P., Xiong, X., Scannail, A. N., Leary, N., Prosper, S., Viswanathan, S., Luna, X., Boix, C. A., James, B. T., Tanigawa, Y., Galani, K., Mathys, H., Jiang, X., Ng, A. P., Bennett, D. A., Tsai, L., & Kellis, M. (2023). Human microglial state dynamics in Alzheimer's disease progression. *Cell*, *186*(20), 4386-4403.e29. https://doi.org/10.1016/j.cell.2023.08.037

Talbot, K. (2014). Brain Insulin Resistance in Alzheimer's Disease and its Potential Treatment with GLP-1 Analogs. *Neurodegenerative Disease Management*, *4*(1), 31–40. https://doi.org/10.2217/nmt.13.73

Ubaldo-Reyes, L. M., Espitia-Bautista, E., Barajas-Martínez, A., Martínez-Tapia, R., Rodríguez-Mata, V., Noriega-Navarro, R., Escalona, R., Castillo-Hernández, J., Pérez-Torres, A., & Navarro, L. (2024). High-Fat Diet-Induced Blood–Brain Barrier Dysfunction: Impact on Allodynia and Motor Coordination in Rats. *International Journal of Molecular Sciences*, *25*(20), 11218. https://doi.org/10.3390/ijms252011218

VectorBuilder | Revolutionize Gene Delivery. (n.d.). https://www.vectorbuilder.kr/vector/Lib241013-1257ykb.html

Weischenfeldt, J., & Porse, B. (2008). Bone Marrow-Derived Macrophages (BMM): Isolation and Applications. *Cold Spring Harbor Protocols*, *2008*(12), pdb.prot5080. https://doi.org/10.1101/pdb.prot5080

Wood, J. I., Ppasia, G., Rolland-Du-Roscoat, P., Desai, S., Choudhury, S., Balbaa, A., Gavriouchkina, D., Blunskyte-Hendley, M., Hardy, J., Cummings, D. M., Salih, D., Hanrieder, J., & Edwards, F. A. (2025). Spatially Resolved Microglial Expression Around

Aβ Plaques in Human Alzheimer's Disease Tissue. *bioRxiv (Cold Spring Harbor Laboratory)*. https://doi.org/10.1101/2025.08.29.673089

Xia, S., Chen, H., & Tang, T. (2023). Risk of Death from Alzheimer's Disease Associated with Brain Tumor, Glioma, and Glioblastoma. *Journal of Alzheimer S Disease*, *96*(2), 623–631. https://doi.org/10.3233/jad-230554

Xu, W., Atti, A., Gatz, M., Pedersen, N., Johansson, B., & Fratiglioni, L. (2011). Midlife overweight and obesity increase late-life dementia risk. *Neurology*, *76*(18), 1568–1574. https://doi.org/10.1212/wnl.0b013e3182190d09

Xu, Z., Peng, B., & Rao, Y. (2021). Microglia replacement by microglia transplantation (Mr MT) in the adult mouse brain. *STAR Protocols*, *2*(3), 100665. https://doi.org/10.1016/j.xpro.2021.100665